Simulation of Injection–Compression-Molding Process. II. Influence of Process Characteristics on Part Shrinkage

SHIA CHUNG CHEN, YUNG CHUNG CHEN, HSIN SHU PENG

Department of Mechanical Engineering, Chung Yuan Christian University, Chung Li, 32023, Taiwan, Republic of China

Received 12 January 1999; accepted 25 June 1999

ABSTRACT: A numerical algorithm is developed to simulate the injection–compression molding (ICM) process. A Hele–Shaw fluid-flow model combined with a modified control-volume/finite-element method is implemented to predict the melt-front advancement and the distributions of pressure, temperature, and flow velocity dynamically during the injection melt filling, compression melt filling, and postfilling stages of the entire process. Part volumetric shrinkage was then investigated by tracing the thermal–mechanical history of the polymer melt via a path display in the pressure–volume–temperature (PVT) diagram during the entire process. Influence of the process parameters including compression speed, switch time from injection to compression, compression stroke, and part thickness on part shrinkage were understood through simulations of a disk part. The simulated results were also compared with those required by conventional injection molding (CIM). It was found that ICM not only shows a significant effect on reducing part shrinkage but also provides much more uniform shrinkage within the whole part as compared with CIM. Although using a higher switch time, lower compression speed, and higher compression stroke may result in a lower molding pressure, however, they do not show an apparent effect on part shrinkage once the compression pressure is the same in the compression-holding stage. However, using a lower switch time, higher compression speed, and lower compression stroke under the same compression pressure in the postfilling stage will result in an improvement in shrinkage reduction due to the melt-temperature effect introduced in the end of the filling stage. © 2000 John Wiley & Sons, Inc. J Appl Polym Sci 75: 1640–1654, 2000

Key words: injection–compression molding; convectional injection; shrinkage; uniform molding pressure

INTRODUCTION

Injection molding,[1] being one of most important polymer processing operations, consists of three major stages: filling, packing, and cooling. As a result of the extensive application of plastics in all areas of industry, there is not only an increasing need for injection molds but also a strong request for high-quality parts in the plastic industry. Part defects such as uneven shrinkage, warpage, sink marks, residual stress, and part mechanical properties may result from the filling, packing, and cooling phases or the entire injection-molding process. Particularly, in the postfilling stage, additional polymer melt is forced into the cavity under a high packing pressure to compensate for subsequent shrinkage due to solidification. This often causes packing pressure loss in the mold cavity and results in nonuniform shrinkage, residual stresses, and severe warpage within the molded parts. To avoid the disadvantages caused by nonuniform packing, two molding processes, namely, gas-assisted injection molding and injec-

Correspondence to: S. C. Chen (shiachun@cycu.edu.tw).

Contract grant sponsor: National Science Council; contract grant number: 85-2216-E033-006.

Contract grant sponsor: Chung Yuan Christian University.

Journal of Applied Polymer Science, Vol. 75, 1640–1654 (2000)

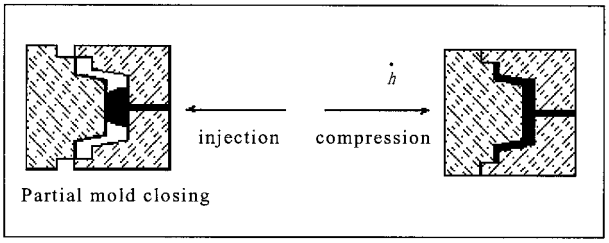

Figure 1 Schematic of ICM process.

tion–compression molding, are considered to be very useful.

In a pure compression-molding process,[1–4] polymer melt is compressed to flow by moving the movable platen of the mold to complete melt filling. The melt is then continued to be compressed by the pressure exerted from the mold wall of the core side. This process provides a more uniform pressure along the cavity wall and requires only a low molding pressure for the postfilling process. Because of this, part warpage and residual stress can be minimized. The most popular application of such a process is SMC compression molding. However, this operation cannot achieve high productivity due to the labor-intensive charge installation. It also has a limitation for molding large parts of complex shape.

Injection–compression molding (ICM),[5–9] combining conventional injection molding and compression molding, was developed to incorporate the advantages of both molding processes. An ICM machine is constructed by modifying an injection-molding machine with an additional compression system. Figure 1 shows a schematic of the ICM process. The compression stage can be introduced after partial melt filling of the cavity. It can also be activated only to replace the packing and holding stages of conventional injection molding (CIM) after melt filling. Generally speaking, the ICM process retains the advantages of CIM, such as high production rate, steady process operation, and easy process automation. Compared with the traditional injection molding, ICM has the following advantages: (1) decreasing molding pressure, (2) reducing residual stress, (3) minimizing molecular orientation, (4) evenly packing, (5) reducing uneven shrinkage, (6) overcoming sink mark and warpage, (7) reducing birefringence, (8) reducing density variation, and (9) increasing dimension accuracy. Because of these advantages, ICM was employed to produce parts of high accurate dimension and free of residual stress especially for the manufacturing of optical parts. Despite the advantages associated with this molding technique, it has introduced new processing parameters and makes the processing control more complex and critical. For example, if the switch from injection to compression and/or compression speed is not properly controlled, it may, on the contrary, cause a high molding pressure and residual stress on the last filled portion of the parts. Although there are several practical cases in industry and some molding experiences in few research groups,[5–14] it is difficult to obtain detailed process information because of confidentiality. Systematic studies regarding to the simulations of polymer melt flow in the ICM process are vary rare[15–18] at the present time. Therefore, the molding window cannot be easily found during the design stage.

In this article,[18] a numerical algorithm is first developed to simulate the non-isothermal melt-filling stage of ICM. The generalized Hele–Shaw flow model combined with a modified control-volume/finite-element (CV/FEM) method is implemented to predict the melt-front advancement and the distributions of cavity pressure, melt temperature, and flow velocity dynamically during the molding process. Simulations were then extended to the postfilling stage, resulting in predictions of the part density distribution using pressure–volume–temperature (PVT) diagrams. By tracing the thermal–mechanical history of a polymer melt via the PVT path display during the entire process, part volumetric shrinkage and the associated distribution can be obtained. A disk part (Fig. 2) was both injection–compression-molded and injection-molded experimentally to verify the simulated molding pressures. Simulations of the ICM process were performed under different processing parameters including com-

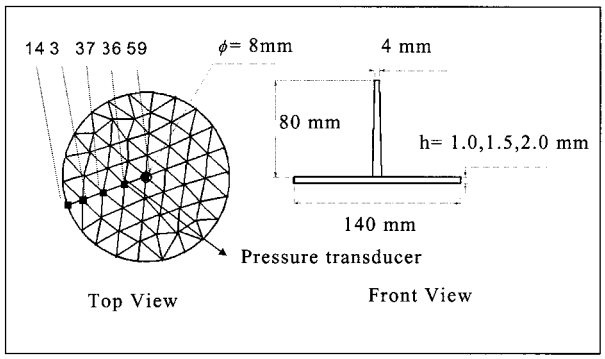

Figure 2 Geometry and triangular element mesh of the disk part.

pression speed, switch time from injection to compression, compression stroke (or initial cavity thickness), and part thickness in order to understand the process characteristics and to determine their influence on the part shrinkage. Simulations were also applied assuming CIM for comparison purposes. Comparison was made at the assumptions of constant flow rate at the filling stage and the same packing pressure at the post-filling stage.

MATHEMATICAL MODELING

Modeling for Melt Filling During Injection Stage

It has been generally accepted that the Hele–Shaw type of flow model provides a reasonably accurate description of polymer melt flow in the three-dimensional thin cavities. As a result, the relevant governing equations for the inelastic, non-Newtonian fluid flow under nonisothermal conditions are similar to those used in CIM[19–23]:

$$0 = \frac{\partial}{\partial z}\left(\eta\frac{\partial u}{\partial z}\right) - \frac{\partial P}{\partial x} \tag{1}$$

$$0 = \frac{\partial}{\partial z}\left(\eta\frac{\partial v}{\partial z}\right) - \frac{\partial P}{\partial y} \tag{2}$$

$$\frac{\partial \rho}{\partial t} + \frac{\partial}{\partial x}(h\bar{u}) + \frac{\partial}{\partial y}(h\bar{v}) = 0 \tag{3}$$

$$\rho C_P\left(\frac{\partial T}{\partial t} + u\frac{\partial T}{\partial x} + v\frac{\partial T}{\partial y}\right) = \frac{\partial}{\partial z}\left(k\frac{\partial T}{\partial z}\right) + \eta\dot{\gamma}^2 \tag{4}$$

where P, T, u, and v represent the pressure, temperature, and melt velocities in the x and y directions, respectively. h is the thickness of mold cavity in the gapwise direction, z. $\bar{u}$ and $\bar{v}$ are averaged velocities gapwisely for u and v, correspondingly. In addition, $\dot{\gamma}$, η, ρ, C_p, and k are the shear rate, viscosity, density, specific heat, and thermal conductivity for the polymer melt. $\bar{u}$ and $\bar{v}$ are averaged velocities gapwisely for u and v, respectively:

$$\bar{u}(x, y) = \frac{1}{h}\int_0^h u(x, y, z)\, dz \tag{5}$$

$$\bar{v}(x, y) = \frac{1}{h}\int_0^h v(x, y, z)\, dz \tag{6}$$

Non-Newtonian characteristics of polymer melt viscosity is described by a form of modified-Cross model with Arrhenius temperature dependence,[19] that is:

$$\eta(T, \gamma) = \frac{\eta_0(T)}{1 + (\eta_0\dot{\gamma}/\tau^*)^{1-n}} \tag{7}$$

with

$$\eta_0(T) = B\,\exp\left(\frac{T_b}{T}\right) \tag{8}$$

During the injection melt-filling and compression melt-filling stages, the compressibility of the polymer melt is neglected; eqs. (1) and (2) can be integrated into eq. (3) and become

$$\frac{\partial}{\partial x}\left(S\frac{\partial P}{\partial x}\right) + \frac{\partial}{\partial y}\left(S\frac{\partial P}{\partial y}\right) = 0 \tag{9}$$

with

$$S = \int_0^h \frac{z^2}{\eta}\, dz \tag{10}$$

Modeling for Melt Filling During Compression Stage

During the compression-molding stage, the relevant equations for the numerical formulation can be modified to be[1]

$$\frac{\partial}{\partial x}\left(-S\frac{\partial P}{\partial x}\right) + \frac{\partial}{\partial y}\left(-S\frac{\partial P}{\partial y}\right) = \dot{\lambda} \tag{11}$$

with $\dot{h} = -dh/dt$, which defines the compression speed, and S is

$$S = \int_0^h \frac{(z - \lambda)^2}{\eta}\, dz \tag{12}$$

λ is the value of z where shear stress vanishes. By assuming the no-slip boundary condition on the cavity wall of the steady platen, λ^1 can be calculated by

$$\lambda = \frac{\int_0^h \frac{z\,dz}{\eta}}{\int_0^h \frac{dz}{\eta}} \tag{13}$$

Equation (9) can be considered as a special case of eq. (11) when $\dot{h}$ is equal to zero.

Modeling for Postfilling Stage

In the postfilling stage, calculation of the melt shrinkage and compressibility of the polymer melt is based on the PVT equation of state by Tait in the form[19] of

$$\nu(P, T) = \nu_0(T)[1 - C \ln(1 + P/B(T))] + \nu_t(T, P) \tag{14}$$

where

$$\nu_0(T) = \beta_1 + \beta_2(T - \beta_5)$$
$$B(T) = \beta_3 \exp[-\beta_4(T - \beta_5)]$$
$$T_t(P) = \beta_5 + \beta_6 P$$
$$\nu_t(P, T) = \beta_7 \exp[\beta_8(T - \beta_5) - \beta_9 P]$$

β_1, β_2, β_3, β_4, β_5, β_6, β_7, β_8, and β_9 are material constants.

Instead of the packing and cooling stages of CIM, after a complete melt-filling stage, compression pressure is applied to the mold cavity by the moving platen in the postfilling stage of the ICM process. As a result, eqs. (1) and (2) can be integrated into eq. (3) and become

$$G(P, T)\frac{\partial P}{\partial t} + \frac{\partial}{\partial x}\left(-S\frac{\partial P}{\partial x}\right) + \frac{\partial}{\partial y}\left(-S\frac{\partial P}{\partial y}\right) = F(P, T) + \frac{\dot{h}}{h} \tag{15}$$

with

$$G(P, T) = \int_0^h \left\{\frac{C}{[B(T) + P][1 - C \ln(1 + P/B(T))]}\right\} dz \tag{16}$$

$$F(P, T) = \int_0^h \left\{\frac{\beta_2}{v_0(T)} - \frac{CP\beta_4}{[1 - C \ln(P/B(T)][B(T) + P]}\right\}\frac{\partial T}{\partial t}\,dz \tag{17}$$

Calculation of the shrinkage index can be considered as the difference of the part specific volume between melt temperatures at ejection and room temperature of 25°C, that is:

$$\text{shrinkage index} = \frac{\nu_e - \nu_r}{\nu_r} \times 100\%$$

where v_r is the specific volume at room temperature 25°C, and v_e, the specific volume at temperature of part ejection.

NUMERICAL ALGORITHM

CV/FEM Method

The CV/FEM technique[19–23] has been become an efficient approach for modeling the flow front progression during the molding process and the calculation of pressure and velocity distribution within the mold cavity filled with the melt. Typical studies can be found in Wang et al.[19] for injection-mold-filling simulation and from Liang[4] for compression-molding simulation.

To construct control volumes used for CV/FEM simulation technique, the part surface is meshed with three-node triangular elements as shown in Figure 2. Part thickness is incorporated into eqs. (11) and (13) during calculation. Note that the thickness of the control volumes will decrease due to the mold closing in the compression-molding stage.

For determining the pressure field during the melt-injection period, eq. (11) of the Laplacian form is described using the standard Galerkin finite-element method.[23] The control volume formulation can also be employed directly to obtain the same described form.[19–23] The net flow, $q_i^{(\ell)}$, which enters its control volume, from an adjacent ℓ can be represented by

$$q_i^{(\ell)} = S^{(\ell)} \sum_{k=1}^{2 \text{ or } 3} D_{ik}^{(\ell)} P_k^{(\ell)} \tag{18}$$

where i is the local index for node A in the element ℓ and $i = 1$, 2, or 3 for triangular elements. The subscript k denotes the local node index in element ℓ and $D_{ik}^{(\ell)}$ is the influence coefficient of the nodal pressure to the net flow in element ℓ. Linear interpolation functions are used. The values of $D_{ik}^{(\ell)}$ are equal to

$$D_{ik}^{(\ell)} = \sum_{1}^{3} \frac{B_i B_k + C_i C_k}{4\Delta^{(\ell)}} \tag{19}$$

In eq. (19), $\Delta^{(\ell)}$ is the area of the triangular element ℓ, $B_1 = y_2 - y_3$, and $C_1 = x_3 - x_2$, where x and y are planar coordinates of the nodes in the triangular element. The other coefficients are obtained by cyclically permuting the subscripts. At the entrance, the net flows from all adjacent elements must satisfy the following relationship:

$$\sum_{\ell'} q_i^{\ell'} = \frac{Q}{2} \tag{20}$$

where Q is the total volumetric flow rate of the polymer melt. For the interior nodes, the net flows from all adjacent elements obey the conservation law of mass are equal to zero, that is:

$$\sum_{\ell'} q_i^{\ell'} = 0 \tag{21}$$

Equations (15) and (18) can be finally integrated and assembled into a matrix form of

$$[K]\{P\} = \{G\} \tag{22}$$

where $[K]$ is the element coefficient matrix; $\{P\}$, the column matrix associated with pressure, P; and $\{G\}$, the column matrix for the variable, G_m $G_m = Q/2$ if m, represented in a global node index number, is the entrance node of the polymer melt. Otherwise, $G_m = 0$.

In addition, boundary conditions at the melt-front boundary, cavity surfaces, and melt inlet region must also be specified. At the melt-front nodes, the nodal pressures are equal to zero (gauge pressure). Along the cavity side wall where the melt is impermeable, the boundary condition is specified as

$$\frac{\partial P}{\partial n} = 0 \tag{23}$$

Since in deriving eq. (18) for nodes located on the cavity side the melt-flow rate across the cavity side wall is assumed to be zero, the boundary condition in the form of eq. (23) is automatically fulfilled. Near the melt entrance region, the boundary conditions are specified according to the operation conditions of the melt. If the pressure is prescribed, then

$$P|_{\text{entrance}} = P_{\text{injection}} \tag{24}$$

and $P_{\text{injection}}$ is the injection pressure at the entrance. If the volumetric flow rate is defined, then the boundary condition is expressed by

$$\oint_C \left(-S\frac{\partial P}{\partial n}\right) ds = \frac{Q}{2} \tag{25}$$

where C is any closed contour lying in the melt-filled region and enclosing the melt entrance. In the present study, the melt-flow rate, Q, is determined from the filling speed during the melt-injection period. As a result, eq. (22) is automatically satisfied when applying eq. (18). To verify the numerical convergence in every step of the analysis, the mass conservation at the melt entrance expressed by eq. (20) is also checked once the pressure and the flow rate $q_i^{(\ell)}$ in each subelement are obtained.

For determining the temperature field, the same method reported previously is used.[19–23] The calculation of the nodal temperature is basically weighted from the subvolumes of all adjacent elements. However, the convection term and the viscous-heating term consider only the contribution of the upstream elements. An implicit method is used for the conduction term, whereas the convection and viscous-heating terms were evaluated at the earlier step. The iteration criteria and algorithm are also similar to those in CIM.[19–23]

Algorithm for Melt-front Advancement During Melt Injection

To distinguish the entrance node and the interior nodes from the melt-front nodes, a filling parameter f is defined and calculated during all analyses. f is equal to 1 for the entrance node and

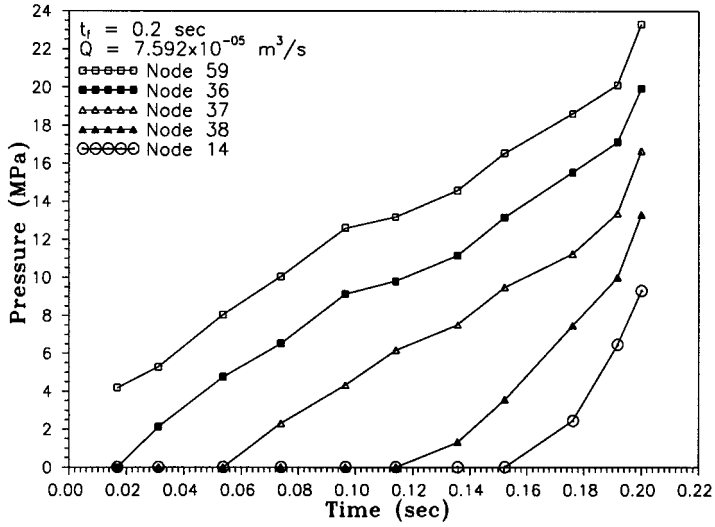

Figure 3 Simulated pressure profiles at different nodes during the melt-filling stage of CIM process.

interior nodes, whereas $0 < f < 1$ for the melt-front nodes. When f is 0, the node is designated as an empty node. At the melt-front nodes, the net flow entering the control volume from neighboring elements which are filled with the melt can be computed. The analysis interval is chosen so that only one melt-front node gets filled per step. Once the pressure field is determined, the gapwise velocity profile for the shear rate values can be calculated. At the melt fronts, a uniform profile for temperature and gap-averaged velocity is assumed to account for the fountain flow effect.

Algorithm for Melt Front Advancement During Melt Compression

The analysis algorithm for compression molding begins with a mass balance on a control volume. The flux of material through the surfaces of the control volume is equal to the induced flow due to mold closure, that is, the volumetric flow rate of material through the surface is equal to the rate at which the closing upper mold displaces a volume previously occupied by the compression process. The mass balance may therefore be written as

$$\int_L \vec{V} \cdot \vec{n}\, dL = Q_c = -\sum_{e=1}^{m} \frac{\dot{h}\Delta_e}{3} \tag{26}$$

where m is the total number of subelements in the melt-filled control volume; Δ_e, the area of the triangular element e; $\vec{v}$, the melt velocity at the melt front surface; and Q_c, the total melt-flow rate introduced by compression. Details can be found elsewhere.[15]

The left-hand side of eq. (26) is the flux of material through the side surfaces of the control volume. Since there is no flow through the upper and lower control volume surfaces which are in contact with the mold, the contribution of these surfaces to the integral in eq. (26) is zero. The right-hand side of eq. (26) is the rate of volume displacement due to mold closing.

The filling parameter, f, associated with each control volume must be also taken the mass flux from moving surface into consideration. For control volumes located on the flow fronts, the filling parameter can be calculated from the occupied volume fraction and the additional volume fraction due to compression during a specified instant. The filling parameters are updated at each time step using the following relation[1]:

$$f_{\text{new}} = \frac{f_{\text{org}} V_{\text{org}} + q\Delta t}{V_{\text{new}}} \tag{27}$$

where f = filling parameter of control volume (f_{new} is the new value; f_{org} is the original value) = melt-filled volume within a control volume (V_{new} is the new value; V_{org} is the original value). q is the computed flow rate into a control volume from the side surfaces.

A variable time step is used so that one unfilled control volume becomes completely filled with the

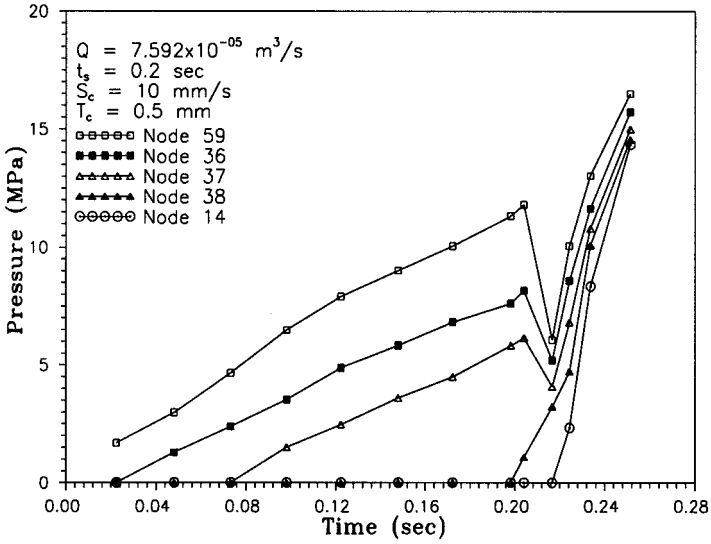

Figure 4 Predicted pressure profiles at different nodes under 10 mm/s compression speed during the melt-filling stage of ICM process.

melt at each time step. To determine the analysis time step, the melt-flow rates into each control volume located on the flow front are computed. Based on these computed flow rates, the unfilled volumes, the filling parameters of the control volumes, and the times needed to fill each control volume can be computed. The smallest value of these filling times is then chosen as the time step for analysis. Once the next node and the associated control volume to be filled has been chosen, the value of Δt is equal to[1]

$$\Delta t = \frac{V_{\text{org}}(1 - f_{\text{org}})}{q + \sum_{e=1}^{m} \frac{\dot{h}\Delta_e}{3}} \tag{28}$$

Correlation of Processing Parameters and Part Geometry

Since the mold cavity is partially open during ICM, the cavity volume is not the same as the final part volume. The injected amount of melt inside cavity before compression must be well defined so that at the end of compression the cavity gap will be exactly the same as the part thickness. Under such circumstances, the compression stroke or initial cavity thickness must be correlated with the switch time from injection to compression. For the flat disk part with a sprue gate, the correlation can be defined as follows: Let V_r be the volume of the sprue; V_p, the disk volume, and T_p, the thickness of disk part; t_f, the filling for purely injection molding, and t_s, the switch time from injection to compression; and S_c, the compression speed. Q is the volumetric flow rate for conventional injection molding and T_c and T_{open} represent the compression stroke and initial cavity thickness, respectively. Then,

$$T_{\text{open}} = T_c + T_p \tag{29}$$

and

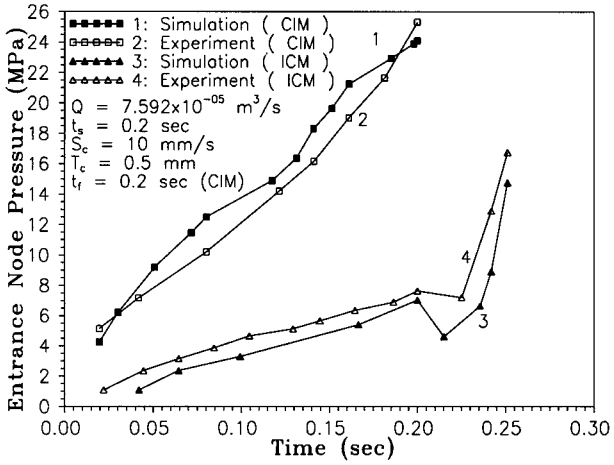

Figure 5 Comparisons of simulated pressure profiles required for ICM and CIM with those obtained from experimental measurements.

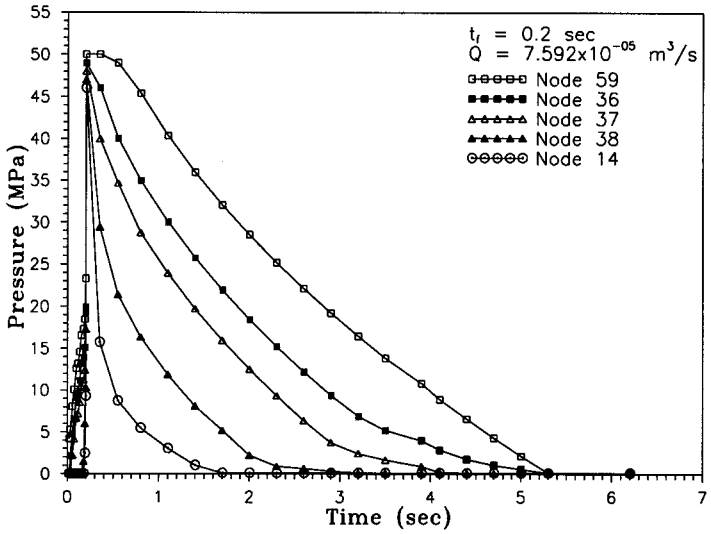

Figure 6 Simulated pressure profiles at different nodes during the entire process of CIM.

$$Q = (V_r + V_p)/t_f \tag{30}$$

Using the same flow rate for comparison purposes, the volume of the cavity filling, V_{melt}, during the melt injection of the ICM process is given by

$$A_{\text{melt}} = (Qt_S - V_r) \tag{31}$$

As a result, the compression stroke, T_c, is then defined as

$$A_{\text{melt}}(T_c + T_p) = V_p \tag{32}$$

where A_{melt} is the occupied melt area within the cavity during the injection stage. From the correlation described above, it is clear that the compression stroke, T_c, is determined by the switch time and the melt-flow rate at the entrance. The latter also depends on the part volume, the runner volume, and the specified filling time required by purely CIM. The total melt-filling time, $t_{f,\text{ICM}}$, then becomes

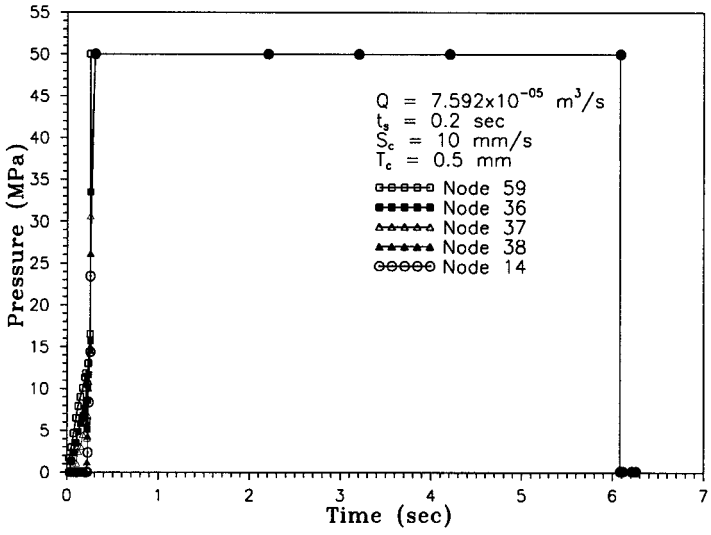

Figure 7 Predicted pressure profiles at different nodes during the entire process of ICM.

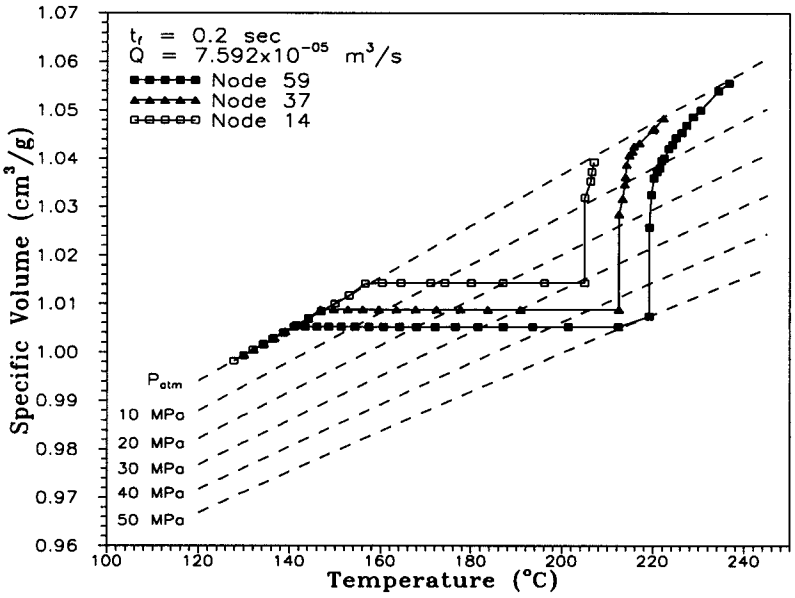

Figure 8 Simulated thermal–mechanical history via path display in PVT diagram for the entrance node during CIM process.

$$t_{f,\mathrm{ICM}} = t_S + T_c/S_c \tag{33}$$

EXPERIMENTS

A 75-ton Battenfeld coinjection-molding machine capable of setting three stages of compression speed was used for the present experiments. A disk part of 140-mm diameter with a thickness of 1.5 mm is both injection-molded and injection–compression-molded using transparent polystyrene (PS). Melt temperatures for the PS resin was 240°C and the mold temperature was 40°C. Filling times for full injection molding were 0.1, 0.2,

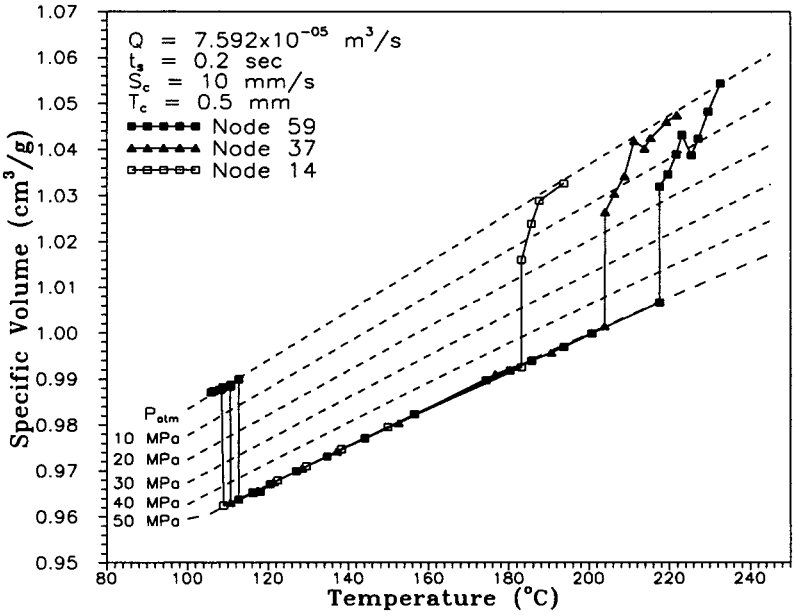

Figure 9 Predicted thermal–mechanical history via path display in PVT diagram for the entrance node during ICM process.

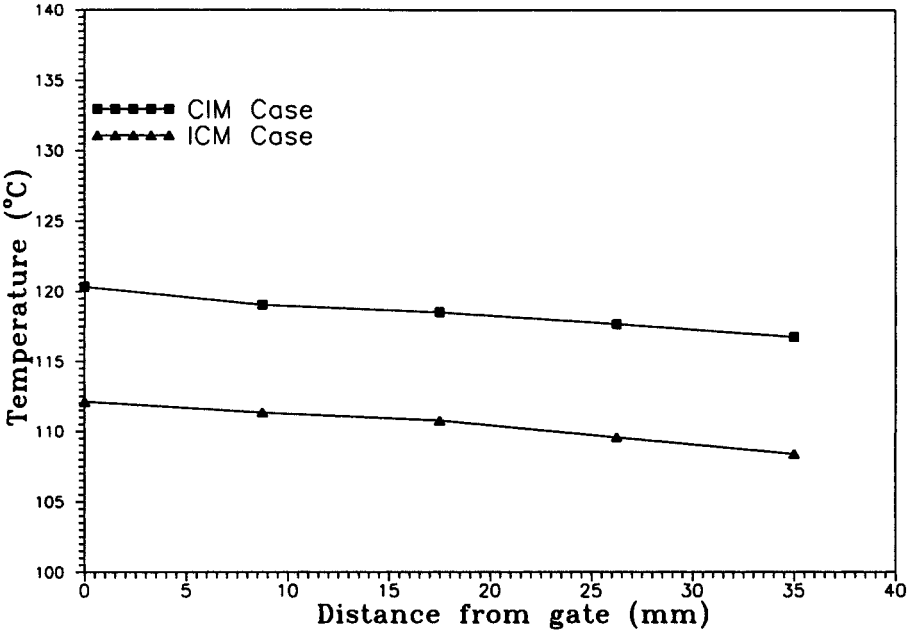

Figure 10 Predicted temperature profiles along radial positions for both CIM and ICM.

and 0.25 s. The postfilling time was 6 s. For ICM, the mold cavity was opened to 2, 2.5, and 3 mm thick. The melt was first injected for a specified period, then the compression molding started. The compression speeds used were 5, 10, and 15 mm/s. A pressure transducer (KISTLER 6159AO type) was installed near the gate (node number 36, Fig. 2). Cavity pressure variations during the molding process were recorded for verification purposes. During the postfilling stage, the holding pressure was set to 50 MPa for both CIM and ICM.

For PS (CHI MEI/PG33), materials constants in the modified-Cross model used for the viscosity values are $n = 0.2838$, $\tau^* = 1.791E + 04$ Pa, $B = 2.591E - 07$ Pa s, and $T_b = 11{,}680$ K[1]. The density, specific heat, and thermal conductivity of PS are 940 kg/m^3, 2100 J/kg K, and 0.18 W/m K, respectively.[1]

SIMULATED RESULTS AND DISCUSSION

Simulated results on the cavity-pressure variations during the melt-filling stage at various locations of the CIM process are depicted in Figure 3. For the simulation of injection–compression, different compression speeds, varying from 5 to 15 mm/s, were assumed. The switch times from melt injection to compression were also varied (0.1, 0.2, and 0.25 s). The packing pressure was assumed to be 50 MPa at the nozzle for ICM and uniformly distributed in the moving platen for the ICM. A typical cavity pressure variation for the injection–compression mold-filling stage under a 10 mm/s compression speed is shown in Figure 4. Compared with CIM, it was found that the required mold-filling pressure of ICM is lower by about 33% and the difference between the maximum and the minimum cavity-pressure values was also lower. To confirm the accuracy of the present numerical predictions, simulated filling pressures required for both injection molding and ICM were verified by cavity pressure measurements. One of these results is shown in Figure 5. Simulated

Table I Comparisons of Shrinkage Index at Different Nodes of CIM and ICM Parts

CIM Case		ICM Case	
Node	Shrinkage Index (%)	Node	Shrinkage Index (%)
59	5.199	59	3.148
37	5.581	37	2.964
14	6.150	14	2.828

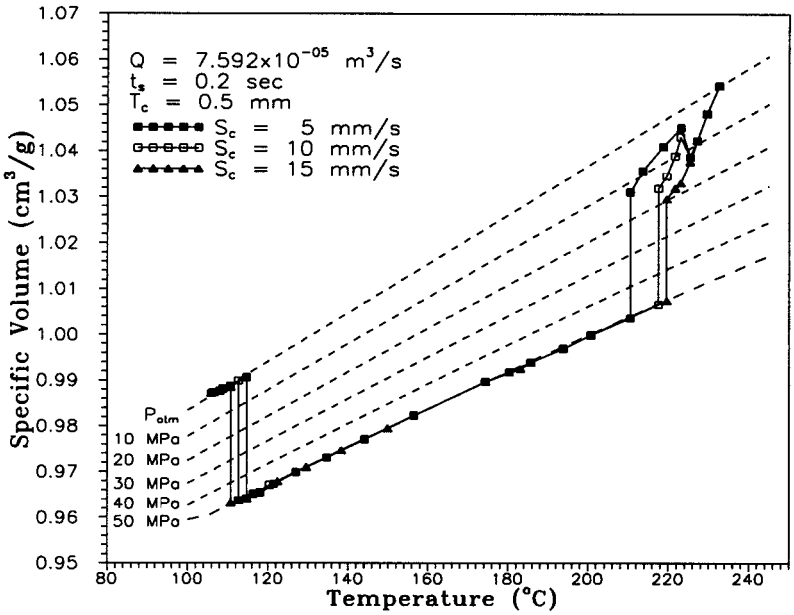

Figure 11 Comparisons of simulated PVT paths for the entrance node under various compression speeds of ICM.

predictions are well consistent with the measured results. A detailed molding-pressure study concerning the influence of processing parameters on the ICM pressure was described elsewhere.[18] Figures 6 and 7 show the pressure distribution of the entire CIM and ICM processes correspondingly. During the postfilling stage of the CIM process, the holding pressure away from gate decreases smoothly as the postfilling stage starts. However, in the ICM process, the compression pressure remains constant until the end of the postfilling process. These two different variations of pressure versus time result in significant differences in thermal–mechanical history displayed via a path for each location in the PVT diagram. The paths of three chosen nodes in the PVT diagram are shown in Figures 8 and 9, respectively, for both CIM and ICM. During the postfilling stage of the CIM process, cavity pressure continues to drop due to the melt cooling until it reaches atmosphere pressure. Then, the melt continues to cool to room temperature. Once the cavity pressure reaches atmosphere pressure, the melt loses contact with the cavity wall and is no longer constrained by the mold. This point is referred as the "ejection point" or called the "detachment point."[24] The melt continues to cool without being confined by the cavity wall.

Location of the detachment point determines the melt volumetric shrinkage. According to Greener,[25] if the melt temperature somewhere inside the mold reaching detachment is still above the T_g, the subsequent cooling without the constraint of the mold wall will lead to uncontrollable shrinkage. The molding will not be geometrically conformable to the cavity. To reduce the melt

Table II Comparison of Shrinkage Index at Different Nodes Under Various Compression Speeds of ICM

ICM Case Sc = 5 mm/s		ICM Case Sc = 10 mm/s		ICM Case Sc = 15 mm/s	
Node	Shrinkage Index (%)	Node	Shrinkage Index (%)	Node	Shrinkage Index (%)
59	3.418	59	3.148	59	2.871
37	3.182	37	2.964	37	2.799
14	2.930	14	2.828	14	2.715

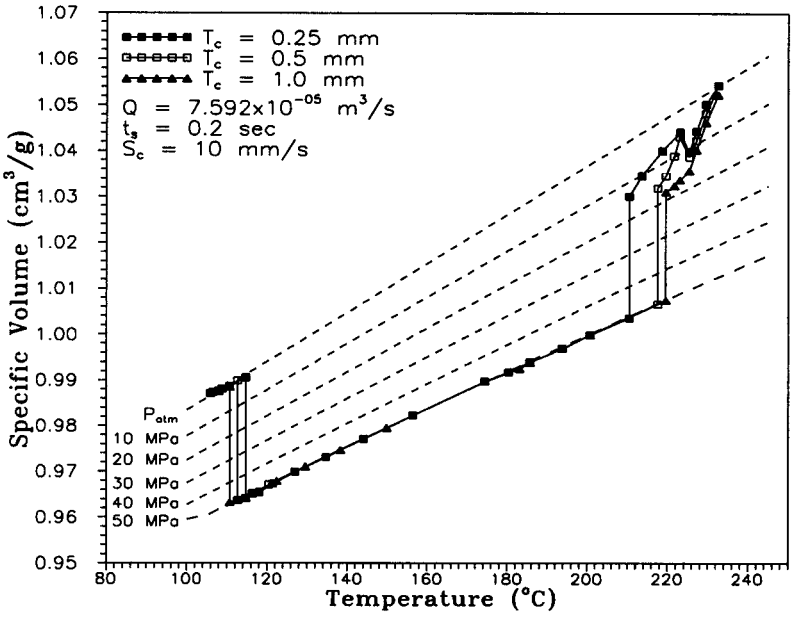

Figure 12 Comparisons of simulated PVT paths for the entrance node under various compression strokes of ICM.

shrinkage, the precision molder usually applies high packing pressures. As shown in Figure 9 for the postfilling stage of the ICM process, the specific volume of the melt at various positions in the cavity decreases with decreasing temperature under almost the same compression pressure until the detachment point is reached. The pressure then drops to atmosphere pressure and the whole part continues to cool to room temperature. Due to the constant and uniform compression pressure held in the postfilling stage of the ICM process, the specific volume at various cavity positions would be much lower and more uniform as compared with the CIM process of which the decay of the cavity pressure was significant. Figure 10 shows the temperature distribution at various cavity positions when reaching the detachment point. According to Figure 10, it can be seen that in the ICM process melt volume shrinkage occurred at lower temperatures and higher pressures. As a result, the shrinkage index should be small or and more uniform when compared with the CIM process (Table I).

Effects of the processing parameters on the shrinkage index were also investigated. Figure 11 shows the PVT paths for the location near the gate (node 59) at various compression speeds of 5, 10, and 15 mm/s. The associated shrinkage index at different locations are listed in Table II. Higher compression speed will result in a decrease in the shrinkage index. The compression speed affects the shrinkage significantly. Figure 12 shows the PVT paths molded at different compression strokes for node 59. The corresponding shrinkage index values at different locations are listed in Table III. Higher compression stroke results in a

Table III Comparison of Shrinkage Index at Different Nodes Under Various Compression Strokes of ICM

ICM Case T_c = 0.25 mm		ICM Case T_c = 0.5 mm		ICM Case T_c = 1.0 mm	
Node	Shrinkage Index (%)	Node	Shrinkage Index (%)	Node	Shrinkage Index (%)
59	2.935	59	3.148	59	3.469
37	2.820	37	2.964	37	3.240
14	2.767	14	2.828	14	2.980

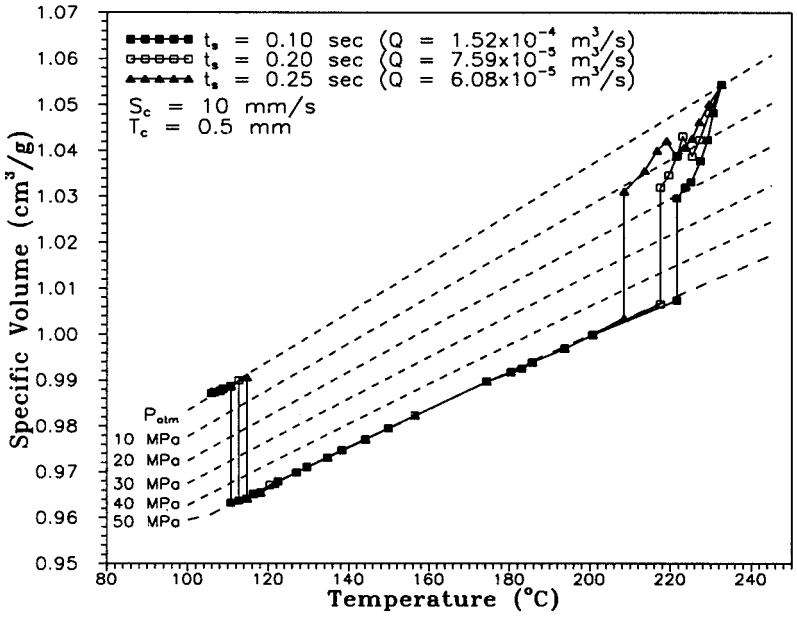

Figure 13 Comparisons of simulated PVT paths for the entrance node under various melt injection rate (associated switch times).

larger shrinkage distribution. For different melt-injection rates corresponding to different switch times, the predicted paths in the PVT curves at the entrance node and shrinkage index variations of different cavity locations are depicted in Figure 13 and Table IV, respectively. It is clear that a lower switch time results in a lower shrinkage distribution. For various part thickness cases, Figure 14 shows the melt-temperature distribution within the cavity when reaching the detachment point. The associated PVT paths at the entrance node and the shrinkage index variations are given in Figure 15 and Table V, correspondingly. It is clear that the thicker part usually results in higher shrinkage values because of the higher melt temperature. In general, when compared with CIM and ICM, ICM provides a uniform and constant compression pressure resulting in lower and more even melt shrinkage. For ICM, the melt temperature and the associated distribution at the end of compression-filling stage determine the melt-shrinkage value and its uniformity. However, various processing parameters including compression speed, compression stroke, switch time, as well as part thickness are the key factors that determine the melt temperature and the associated temperature distribution at the end of the melt-filling process.

CONCLUSIONS

In the present study, a numerical algorithm is developed to simulate the injection–compression process. The Hele–Shaw fluid model combined with the modified CV/FEM is implemented to pre-

Table IV Comparison of Shrinkage Index at Different Nodes Under Various Melt-injection Rates (Associated Switch Times)

ICM Case t_s = 0.1 s		ICM Case t_s = 0.2 s		ICM Case t_s = 0.25 s	
Node	Shrinkage Index (%)	Node	Shrinkage Index (%)	Node	Shrinkage Index (%)
59	2.798	59	3.148	59	3.173
37	2.689	37	2.964	37	3.044
14	2.570	14	2.828	14	2.879

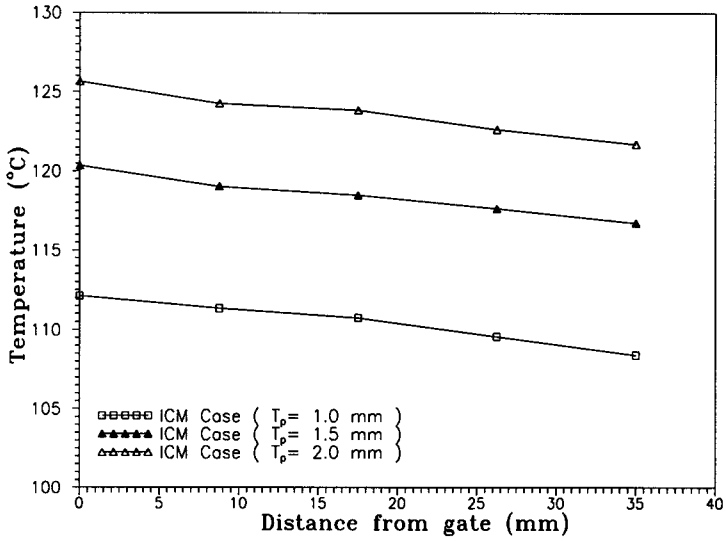

Figure 14 Predicted temperature profiles at various positions for ICM parts of various part thickness.

dict the melt-front advancement and the distributions of pressure, temperature, specific volume, and shrinkage index dynamically during the molding process. Influence on the melt-shrinkage characteristics was investigated by changing the processing parameters including compression speed, switch time from injection to compression, compression stroke, and part thickness. Comparison of the melt shrinkage was also made between the CIM and CIM parts. It was found that

1. The thermal–mechanical history of the molding process displayed via the path in the PVT diagram can be used to present melt shrinkage. Location of the detach-

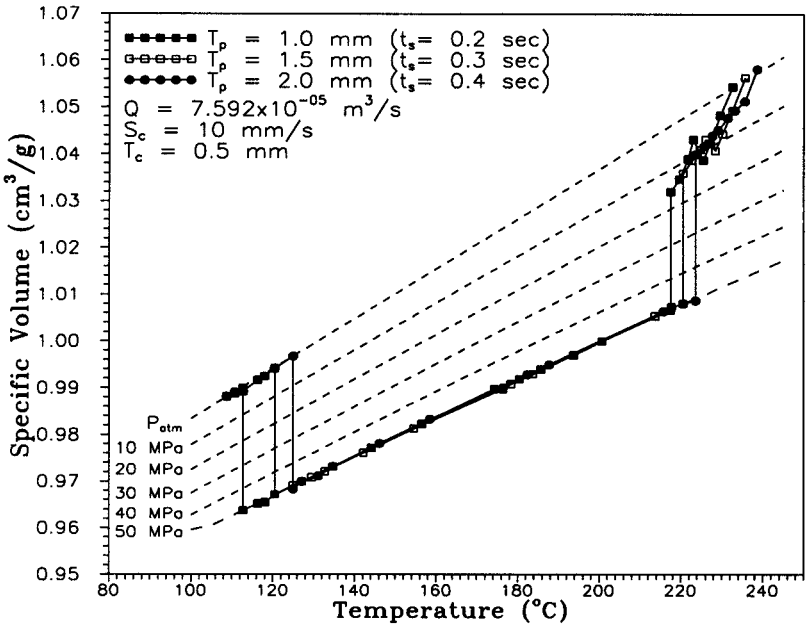

Figure 15 Comparisons of simulated PVT paths for the entrance node under various ICM part thickness.

Table V Comparison of Shrinkage Index at Different Nodes for Various Part Thicknesses

ICM Case T_P = 1.0 mm		ICM Case T_P = 1.5 mm		ICM Case T_p = 2.0 mm	
Node	Shrinkage Index (%)	Node	Shrinkage Index (%)	Node	Shrinkage Index (%)
59	3.148	59	3.586	59	3.854
37	2.964	37	3.366	37	3.634
14	2.828	14	3.141	14	3.414

ment point in the PVT diagram determines the final volumetric part shrinkage.

2. For CIM, the packing pressure decreases within the mold cavity in the postfilling stage, leading to larger melt shrinkage and uneven shrinkage distribution. On the other hand, the uniform and constant compression pressure of the ICM results in lower melt shrinkage and even shrinkage distribution.
3. For ICM, the melt temperature and its distribution in the part at the end of filling stage determine the melt shrinkage and shrinkage uniformity. Part thickness, compression speed, compression stroke, and switch time all show different effects on the melt temperature, the final shrinkage, and the shrinkage evenness. In the present study, faster compression speed, smaller compression stroke, smaller switch time, and a thinner part result in lower part shrinkage and better shrinkage uniformity.

This research was supported by the National Science Council under NSC Grant 85-2216-E033-006 and the Distinguished Research Grant of Chung Yuan Christian University.

REFERENCES

1. Isayev, A. I.; Upadhyay, R. K. In Injection and Compression Molding Fundamentals; Marcel Dekker: New York, 1987.
2. Lee, C. C.; Castro, J. M. In Fundamentals of Computer Modeling for Polymer Processing; Tucker, C. L., III, Ed.; Hanser: New York, 1989.
3. Lee, L. J.; Fan, J. D. Int Polym Proc 1991, 6, 61–72.
4. Liang, E. W. Polym Compos 1995, 16, 70–82.
5. Klepek, G. Kunststoffe 1987, 77, 13–26.
6. Abe, T.; Tanaka, T. Polymer Application Development Laboratory, I. P. Co. Ltd., Asia Regional Meeting of PPS, 1991.
7. Friedrichs, B.; Friesenbichler, W.; Gissing, K. Kunststoffe 1990, 80, 583–591.
8. Huang, T. Y.; Chen, C. T.; Hsieh, J. R. Internal Report of Material Industry Development Center, 1993.
9. Takeo, I.; Kenzi, Y. Internal Report of Takeo IMURA Machinery Works Co., Ltd., 1992.
10. Young, S.; Ke, M. K. SPE Tech Pap 1993, 39, 2188–2191.
11. Young, S.; Ke, M. K. SPE Tech Pap 1993, 39, 2182–2187.
12. Haufer, H.; Berlin, G. F. Kunststoffe 1989, 79, 15–16.
13. Munich, K. K. Kunststoffe 1987, 77, 22.
14. Knappe, W.; Lampll, A. Kunststoffe 1984, 74, 7.
15. Chen, Y. C.; Chen, S. C.; Chang, M.; Ho, C. S. Chung Yuan J 1996, 24, 1.
16. Wang, T. J. ASME 1997, 79, 83–95.
17. Wang, T. J. Proceeding of the C-MOLD Asia-Pacific Users' Conference, Hsinchu, Taiwan, ROC, March 11–13, 1997; Vol. 2, p 9.
18. Chen, S. C.; Chen, Y. C.; Cheng, N. T.; Huang, M. S. Int Commun Heat Mass Trans 1988, 25, 907–917.
19. Wang, V. W.; Hieber, C. A.; Wang, K. K. J Polym Eng 1986, 72, 1–45.
20. Chen, S. C.; Pai, P.; Hsu, C. SPE Tech Pap 1988, 34, 250–254.
21. Hsu, K. F. Master Thesis, Chung Yuan University, Taiwan, 1994.
22. Chiang, H. H. Technical Report of Cornell University, Ithaca, 1989; Vol. 62.
23. Huebner, K. H.; Thornton, E. A. In The Finite Element Method for Engineers; Wiley: New York, 1982; Chapters 4 and 5.
24. Yang, S. Y.; Ke, M. Z. Adv Polym Tech 1995, 14, 15–24.
25. Greener, J. Polym Proc 1990, 238, 9.